INTERNATIONAL JOURNAL FOR NUMERICAL METHODS IN FLUIDS, VOL. 22, 67–79 (1996)

A KARHUNEN–LOÈVE ANALYSIS OF TURBULENT THERMAL CONVECTION

I. HAKAN TARMAN

Department of Mathematical Sciences, King Fahd University of Petroleum and Minerals, Dhahran 31261, Saudi Arabia

SUMMARY

The Karhunen–Loève (K–L) procedure is applied to a turbulent thermal convection database which is generated numerically through integration of the Boussinesq equation in a periodic box with stress-free boundary conditions using a Fourier collocation spectral method. This procedure generates a complete set of mutually orthogonal functions in terms of which the turbulent flow fluctuation field is represented optimally in the mean square sense. A study is performed ranging from the direct projection of the database onto the set, resulting in a considerable data compression, to developing a system of dynamical equations employing the set as a basis for approximating the Boussinesq equation. In the latter a new strategy is proposed and tested for the treatment of the mean component of the turbulent flow. Finally, the direct projection and the dynamical equations are used to study the effects of truncation on the representation of the turbulent flow.

KEY WORDS: Karhunen–Loève decomposition; turbulent thermal convection

1. INTRODUCTION

A turbulent flow involves many scales of motion. This sets the basic requirement that a direct numerical simulation must meet if it is to represent turbulence. All scales must be adequately resolved by the computational mesh. This, together with the requirement that a large sample of the set of all possible motions allowed by the governing equation is necessary to provide an adequate statistical evaluation, results in a vast database to be generated through the simulation for subsequent analysis and assessment.

A technique based on the Karhunen–Loève (K–L) procedure[1] has been used extensively in extracting essential features of the flow hidden within the database. These features are then used as a basis in subsequent data compression and model reduction schemes. Some applications range from data compression in turbulent thermal convection[2] to model reduction in the Ginzburg–Landau (G–L) equation[3] and in a turbulent boundary layer.[4]

The application of this procedure to the stochastic turbulent field was proposed by Lumley[5] as a rational and quantitative method, referred to as principal orthogonal decomposition (POD), for extraction of organized structures from the field. New perspectives on the applications of the technique are presented in Reference 6. The technique is based on the decomposition of the turbulent flow fluctuation field into a weighted sum of mutually orthogonal eigenfunctions of the two-point correlation tensor which meet the boundary conditions and appropriate side conditions. This decomposition is unique and optimal in the sense that the random variables appearing as weights in the representation are statistically orthogonal and the mean square error resulting from the truncated representation of the flow is minimized. The energy retained in the truncated representation of the flow is maximized by ordering the eigenfunctions in the representation based on the corresponding

CCC 0271–2091/96/010067–13

Received June 1994
Revised May 1995

eigenvalues, which are interpreted as indicating the average energy of the flow along the direction of the eigenfunctions. This representation will be referred to as the K–L representation of the turbulent flow.

As a consequence of the optimality of the decomposition, the first several terms in the K–L representation often contain a large fraction of the flow energy as a number of problems[2,4] in turbulent flow have shown. The flow can then be satisfactorily approximated by its truncated K–L representation if one is interested in retaining only the energy-containing components of the flow. On the other hand, information regarding the less energetic components associated with the small scales of the flow will be lost through this truncation based on the energy criterion. Application-oriented modifications on the condition of optimality in the K–L procedure have been used in some studies.[7,8]

In the present investigation the K–L procedure is applied to a numerically generated database. For this purpose the Boussinesq equation governing thermal convection is numerically integrated in a periodic box with hot lower and cold upper free surfaces under conditions that result in turbulent flow. The integration is performed using a Fourier collocation spectral method. Some earlier numerical studies of turbulent thermal convection can be found in References 2, 9 and 10 and references cited therein. A substantial compression in turbulence data is achieved through the K–L representation of the flow field. The effects of truncation are demonstrated on the flow reconstructed from its truncated K–L representation. In addition, a second database is generated through the numerical integration of the K–L-based dynamical system approximating the Boussinesq equation to demonstrate the effects of truncation in a dynamical environment as well as to test a new strategy presently proposed for the treatment of the mean component of the flow in such a dynamical approximation. This work is an extension of an earlier study reported in Reference 2.

2. THE KARHUNEN–LOÈVE PROCEDURE

In the context of turbulence this procedure is a result of the search for the most similar structure ψ in the mean square sense to an ensemble of, say, realizations of a statistically time-stationary turbulent flow $\mathbf{v}(\mathbf{x})$ on a domain Ω. The search results in ψ satisfying the integral equation

$$\int_{\Omega} \mathbf{R}(\mathbf{x}, \mathbf{x}')\psi(\mathbf{x}')d\mathbf{x}' = \lambda\psi(\mathbf{x}) \tag{1}$$

whose kernel is the two-point correlation tensor $\mathbf{R}(\mathbf{x}, \mathbf{x}') = \langle \mathbf{v}(\mathbf{x}) \otimes \mathbf{v}(\mathbf{x}') \rangle$ The brackets $\langle . \rangle$ denote ensemble averaging and $\otimes$ denotes a dyadic product. For the bounded domain Ω the square integrability of the flow $\mathbf{v}$, thus of $\mathbf{R}$, and the symmetry of the kernel $\mathbf{R}$ assure us through the Hilbert–Schmidt theory that there are a countably infinite number of solutions to (1) forming a complete set of orthogonal functions $\{\psi^n(\mathbf{x})\}$ in terms of which the flow may be decomposed as

$$\mathbf{v}(\mathbf{x}) = \sum_n a_n \psi^n(\mathbf{x}). \tag{2}$$

The index n refers to a member of the set $\{\psi^n(\mathbf{x})\}$ which is ordered with respect to the decreasing eigenvalues $\lambda_n \geqslant \lambda_{n+1} \geqslant \cdots$, which are guaranteed to be non-negative, $\lambda_n \geqslant 0$, by the non-negative definiteness of $\mathbf{R}(\mathbf{x}, \mathbf{x}')$. The decomposition in (2) is unique in the way that the mean square error resulting from a truncated representation is a minimum among other possible orthogonal decompositions of the flow in the form of (2) and that the random expansion coefficients a_n are statistically orthogonal,

$$\langle a_n a_m^* \rangle = \lambda_n \delta_{nm}, \tag{3}$$

where superscript * indicates a complex conjugation.

3. THE RAYLEIGH–BÉNARD PROBLEM

3.1. Governing equations

This is the classic problem of the evolution of fluid heated from below in the presence of gravity. The mathematical model which governs this problem is the Boussinesq equation given in the standard normalization[11] by

$$\nabla \cdot \mathbf{u} = 0, \tag{4a}$$

$$\frac{\partial \mathbf{u}}{\partial t} + \mathbf{u} \cdot \nabla \mathbf{u} = -\nabla p + Ra\ Pr\ T\mathbf{e}_z + Pr \Delta \mathbf{u}, \tag{4b}$$

$$\frac{\partial T}{\partial t} + \mathbf{u} \cdot \nabla T = w + \Delta T, \tag{4c}$$

where $\mathbf{u} = [u, v, w]$ represents the velocity in the directions $\mathbf{x} = [x, y, z]$ respectively, T represents the deviation from the linear conduction profile $-\beta z$, p is the pressure and $\mathbf{e}_z$ is the unit vector in the vertical z-direction opposite to gravity. The two dimensionless parameters in (4) are the Rayleigh number $Ra = g\beta H^4 \alpha / \kappa \nu$ and the Prandtl number $Pr = \nu / \kappa$.

The system of equations (4) is considered over the spatial region Ω: $0 \leqslant x, y \leqslant A$, $0 \leqslant z \leqslant 1$, with stress-free boundary conditions (the so-called free–free case)

$$w = T = \frac{\partial u}{\partial z} = \frac{\partial v}{\partial z} = 0 \quad \text{at } z = 0, 1 \tag{5}$$

in the vertical direction and periodic boundary conditions in the horizontal x- and y-directions with period A, where A is the aspect ratio L/H.

3.2. Numerical procedure

These equations are numerically integrated by means of a Fourier collocation spectral method. For this purpose the flow $\mathbf{v} = [\mathbf{u}, T]$ is approximated by a truncated expansion in the form

$$\mathbf{v}_\alpha(\mathbf{x}, t) \approx \sum_{|k_x| \leqslant \frac{1}{2}N_x} \sum_{|k_y| \leqslant \frac{1}{2}N_y} \sum_{k_z = 0}^{N_z} \hat{v}_\alpha(k_x, k_y, k_z; t) V_\alpha^k(\mathbf{x}), \tag{6}$$

where $\mathbf{V}^k(\mathbf{x})$ refers to the orthogonal Fourier basis functions satisfying the boundary conditions and k refers to the integer wave numbers (k_x, k_y, k_z). This approximation is substituted into (4) to yield a system of ODEs for $\hat{v}_\alpha$. The resulting system is then numerically integrated in time. For details on the numerical procedures the reader is referred to Reference 2 and references cited therein.

The integration is performed for the parameter values $Pr = 0{\cdot}72$ and $Ra = 15Ra_c$, where the critical Rayleigh number is $Ra_c = 27\pi^4/4$. The aspect ratio A is taken as $2\sqrt{2}$, corresponding to the wavelength of maximum linear instability.[11] All relevant spatial scales are resolved with the choice of $N_x = N_y = N_z = 20$.

The flow $\mathbf{v}$ is computed from a set of initial conditions taken from a previous study,[2] until the flow quantities reach a statistically nearly stationary state. Then it is sampled at regular intervals to generate a database of 500 time samples, which are estimated to be uncorrelated, adequately representing the flow for the subsequent analysis.

For the flow represented by the ensemble of time samples, the Nusselt number is found to be 3·938. The box-averaged values of the Taylor microscale Reynolds number and mixed temperature skewness, both based on the horizontal velocity, are 11·34 and 0·228 respectively. These values indicate that the

flow is weakly turbulent in nature and this is in agreement with the simulation in Reference 9. The ensemble average is evaluated by a horizontal average over the x–y plane followed by a temporal average over the database.

4. THE KARHUNEN–LOÈVE REPRESENTATION

The flow is decomposed into mean and fluctuating components

$$\mathbf{v} = \langle \mathbf{v} \rangle + \mathbf{v}', \tag{7}$$

where $\langle \mathbf{v} \rangle = [\mathbf{0}, T^0(z)]$ and $\mathbf{v}' = [\mathbf{u}, \theta]$. Subsequently, $\mathbf{v}'$ is used to form the two-point correlation kernel in (1) after its mechanical and thermal components have been rescaled based on the scalings $\sqrt{(Ra\ Pr/2\ Nu)}\kappa/H$ and $\sqrt{(2\ Nu^3/Ra\ Pr)}\beta H$ respectively. This new scaling follows from the physical arguments in Reference 2. The eigenproblem (1) is then solved using the direct method.[6] The computation is significantly simplified using the symmetries of the flow, such as translational invariance in the horizontal directions and the discrete symmetries[2] due to the geometry of the spatial domain.

As an immediate consequence of the translational invariance, each eigenfunction takes the form

$$\boldsymbol{\psi}^k(\mathbf{x}) = \phi^{(q)}(k_x, k_y; z) \exp\left(2\pi \mathrm{i} \frac{k_x x}{A}\right) \exp\left(2\pi \mathrm{i} \frac{k_y y}{A}\right), \tag{8}$$

with the corresponding eigenvalue now represented in the form $\lambda_k = \lambda^{(q)}(k_x, k_y)$, where $k = (k_x, k_y, q)$ and q is the vertical quantum number. The eigensolutions come with a maximum degeneracy of eight, i.e.

$$\lambda^{(q)}(\pm k_x, \pm k_y) = \lambda^{(q)}(\pm k_x, \mp k_y) = \lambda^{(q)}(\pm k_y, \pm k_x) = \lambda^{(q)}(\pm k_y, \mp k_x), \tag{9}$$

owing to the discrete symmetries. The corresponding eigenfunctions are related through the symmetry relations preserving the mutual orthogonality.

There is actually a real flow $\mathbf{v}^k$ associated with each eigenfunction corresponding to a conjugate pair of modes k and k^*, referring to (k_x, k_y, q) and $(-k_x, -k_y, q)$ respectively, satisfying the boundary conditions (5) and the continuity (4a) and represented by

$$\mathbf{v}^k(\mathbf{x}, t) = a_k(t)\boldsymbol{\psi}^k(\mathbf{x}) + a_{k^*}(t)\boldsymbol{\psi}^{k^*}(\mathbf{x}), \tag{10}$$

where $\boldsymbol{\psi}^{k^*} = (\boldsymbol{\psi}^k)^*$ and $a_{k^*} = a_k^*$. The expansion coefficients a_k are evaluated through the inner product $(.,.)$ defined as

$$a_k(t) = (\mathbf{v}', \boldsymbol{\psi}^k) = \int_\Omega v'_\alpha(\mathbf{x}, t)(\psi^k_\alpha(\mathbf{x}))^* \, \mathrm{d}\mathbf{x}, \tag{11}$$

with the summation convention on α. These basic flows in turn act as building blocks and contribute to the building of the flow

$$\mathbf{v} = \sum_k \mathbf{v}^k, \tag{12}$$

where k runs through the conjugate pairs of K–L modes.

Table I. Eigenvalues for first 10 degenerate K–L modes

n	(k_x, k_y, q)	Eigenvalue	Degeneracy	% energy
1	0 1 1	1·0000	4	54·44
2	1 1 1	0·2528	4	13·76
3	0 1 2	0·0668	4	3·64
4	0 0 1	0·0370	1	0·50
5	1 2 1	0·0353	8	3·84
6	0 2 1	0·0338	4	1·84
7	0 1 3	0·0312	4	1·70
8	0 2 2	0·0281	4	1·53
9	0 0 2	0·0257	2	0·70
10	0 3 1	0·0221	4	1·20

4.1. K–L modes

Table I lists the first 10 eigenvalues, each scaled by the largest eigenvalues. Since the total mean energy $\mathscr{E}$ is given by the sum of the eigenvalues

$$\langle(\mathbf{v}', \mathbf{v}')\rangle = \mathscr{E} = \sum_n \lambda_n, \tag{13}$$

each eigenvalue is listed with the fraction of energy associated with it. The first four, not counting the degeneracies, account for more than 70% of the energy. Figure 1 shows the vertical spatial structures $\boldsymbol{\phi}^{(q)}(k_x, k_y; z)$ of the corresponding eigenfunctions. They clearly carry the character of the flow, as shown by the satisfaction of the boundary conditions and the continuity, the symmetry (or antisymmetry) about the midplane and the visible boundary layer and the flat central region. The vertical velocity and temperature components have equal parity; they are both symmetric or antisymmetric about the midplane. The horizontal and vertical velocity components have opposite parities, since their spatial structures are connected through the continuity. In general the

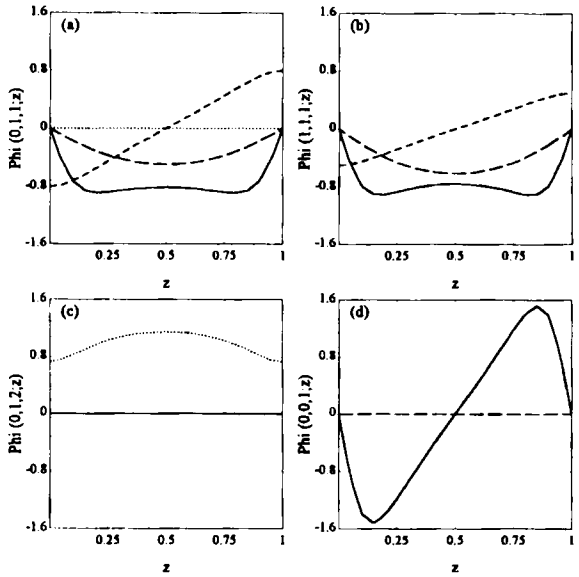

Figure 1. Vertical structure of K–L eigenfunctions $\boldsymbol{\phi}^{(q)}(k_x, k_y; z)$ ($\cdots$, ϕ_1; - - -, ϕ_2; – – –, ϕ_3; ——, ϕ_4): (a) $\boldsymbol{\phi}^{(1)}(0, 1; z)$; (b) $\boldsymbol{\phi}^{(1)}(1, 1; z)$; (c) $\boldsymbol{\phi}^{(2)}(0, 1; z)$; (d) $\boldsymbol{\phi}^{(1)}(0, 0; z)$

eigenfunctions for a given (k_x, k_y) are observed to exhibit an increasing number of zero crossings (sequency) with q.

The flow associated with the first K–L mode is in the form of two-dimensional convective rolls of wavelength A. This can be seen in Figure 1(a) in that the magnitude of the vertical velocity reaches its peak in the midplane where the horizontal velocity is zero. In the upper and lower free surfaces, on the other hand, the magnitude of the horizontal velocity reaches its peak while the vertical velocity is zero. The temperature profile exhibits peaks outside the core region and the visible boundary layers. The mode is fourfold degenerate and the degeneracy arises because the rolls can align with either x- or y-axes corresponding to the flows $\mathbf{v}^{(0,1,1)}$ and $\mathbf{v}^{(1,0,1)}$ as in (10) respectively. The second K–L mode has a similar vertical spatial structure as shown in Figure 1(b) (the horizontal velocity components coincide) and represents a flow in the form of two-dimensional convective rolls of wavelength $A/\sqrt{2}$. These rolls, represented by $\mathbf{v}^{(1,1,1)}$ and $\mathbf{v}^{(1,-1,1)}$, are aligned with the horizontal diagonals of the periodic box as determined by the horizontal wave numbers k_x and k_y. The two modes hold a total of about 68% of the total energy. They are driven by the release of gravitational energy resulting from the heated fluid moving up and cooled fluid moving down.

The third K–L mode, associated with (0, 1, 2), represents a flow of purely shearing motion with no vertical velocity component as shown in Figure 1(c). It is the first energetic mode with a non-vanishing vertical vorticity component. In the absence of vertical velocity its motion can only be sustained by non-linear interactions with the other modes. This is consistent with the fact that the non-linear terms in the equation of motion are responsible for the generation of vertical vorticity.[12] In the Boussinesq equation (4) the vertical velocity provides the active coupling between the mechanical and thermal components of the flow. This is reflected in the K–L modes where those eigenfunctions with no vertical velocity component are purely mechanical, involving only the horizontal components of velocity, or purely thermal. Purely thermal modes appear only in the family of (0, 0, q) modes that are allowed to be onefold degenerate under the discrete symmetries of the flow.

The continuity (4a) and the boundary conditions imply that the horizontal average of the vertical velocity component is identically zero at each instant of time and at any vertical location. As a consequence, all (0, 0, q) modes lack the vertical velocity component and appear either purely mechanical or purely thermal, characterized by twofold and onefold degeneracy respectively. These modes represent the temporal variation about the mean flow $\langle \mathbf{v} \rangle$. As shown in Figure 1(d), the fourth K–L mode (0, 0, 1) represents a onefold degenerate, purely thermal background flow.

4.2. Data compression

For the Fourier representation of the flow in the form of (6), only three components of $\hat{\mathbf{v}}$ need to be saved for each (k_x, k_y, k_z) at each instant, because the velocity components of $\hat{\mathbf{v}}$ are related through the continuity (4a). However, the K–L representation (10)–(12) requires only a_k to be saved for each (k_x, k_y, q) at each instant.

In order to demonstrate data compression, the K–L representation is compared with the Fourier representation of the flow in view of their ability to capture energy in respective truncations involving a given number of saved constants. The average energy capture in the K–L representation is given by the corresponding eigenvalue λ_k for each set of degenerate modes (k_x, k_y, q) as in (9). In order to facilitate the comparison, the energy capture in the Fourier representation is maximized by including the Fourier modes in the order based on the magnitude of the energy averaged over the modes associated with each (k_x, k_y, k_z), such as the degenerate modes in (9) in which k_z is replacing q.

Figure 2 shows the average energy capture in the K–L and Fourier representations versus the number of saved constants at any instant of time. Each is scaled by the total mean energy $\mathscr{E}$ of (13). It is clear from Figure 2 that the K–L representation of the flow is optimal in that it captures more energy in the

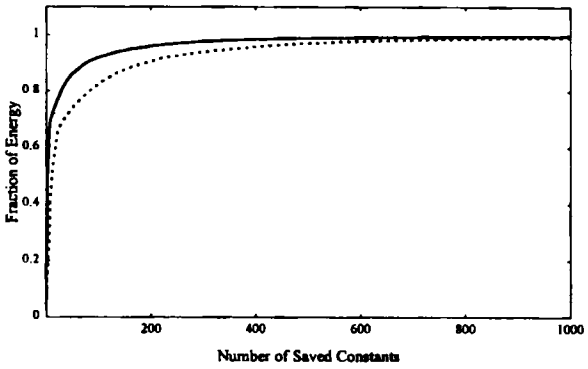

Figure 2. Fraction of energy content in both K–L (—) and Fourier (· · ·) representations of flow involving a given number of saved constants

truncated representation involving a given number of saved constants. This is indicated by the rapid rise in the full curve. However, the later rise in both curves is slow, which indicates that a considerable number of additional terms are required for further improvement in the energy capture in both representations. For example, in the Fourier representation an 80% energy capture requires 90 constants to be stored, while 90% and 99% energy captures require 198 and 891 constants to be stored respectively. On the other hand, the same amounts of energy capture in the K–L representation require 29, 80 and 518 constants to be stored respectively. Thus the K–L representation is indistinguishable from the Fourier representation in terms of the energy capture as far as less energetic higher-order modes are concerned and the efficiency of the K–L representation is apparent only for the energetic features of the flow.

4.3. Convergence

It is clear from the resulting data compression that the K-L representation is optimal in capturing energy for a given truncation. However, this is not expected to hold in general for other quantities that can be constructed from the truncated K–L representation of the flow in the form

$$\mathbf{v}'^{N} = \sum_{k=1}^{N} \mathbf{v}^{k}, \tag{14}$$

where the index k runs through the first N conjugate pairs of modes. In Figure 3 the convergence of certain physically relevant quantities constructed using (14) is shown in the mean square norm $\langle(.,.)\rangle$ versus N. The norm of each quantity is normalized.

Figure 3 shows the convergence of the convective heat transport $\langle(w, \theta)\rangle$. This quantity stands for the production term in the energy equation. Its convergence is remarkably fast when compared with the convergence of the optimally represented quantity, namely energy $\langle(\mathbf{v}', \mathbf{v}')\rangle$, in the same figure. This is also observed in another application[13] where the first few energetic K–L modes contribute substantially to turbulence production. On the other hand, for quantities such as the horizontal, ω_1 (or ω_2), and vertical, ω_3, components of vorticity, where $\omega_i = (\nabla \times \mathbf{u})_i$, which are associated with the small scales of the flow, inclusion of a large number of modes is necessary for a satisfactory construction as shown in Figure 3. Note that the vorticity components involve spatial derivatives of the flow and it is known[14] that the spatial derivatives have an amplifying effect on the importance of the higher-order K–L modes in the representation. Thus the K–L representation provides a scale separation, with the lower-order modes contributing to the large-scale and the higher-order modes to

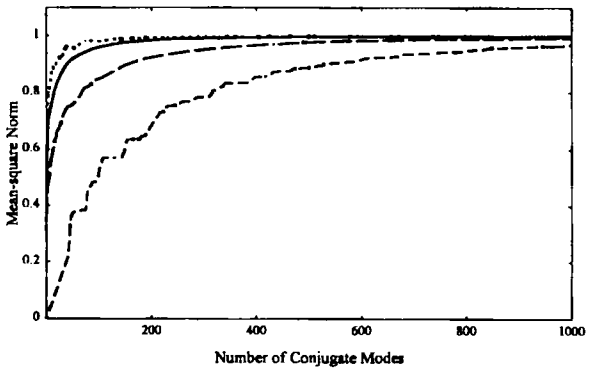

Figure 3. Convergence of normalized mean square norm of some flow quantities in K–L representation ($\cdots$, $\langle w, \theta \rangle$); —, $\langle (\mathbf{v}', \mathbf{v}') \rangle$; - - -, $\langle (\omega_1, \omega_1) \rangle$; - · -, $\langle (\omega_3, \omega_3) \rangle$)

the small-scale features of the flow. The relatively poor convergence of the vertical vorticity is due to the K–L representation of the flow being dominated by the energetic horizontal rolls.

These mean square convergence rates are reflected in the vertical profiles $\langle \omega\theta \rangle$, $\langle \omega_1^2 \rangle^{1/2}$ and $\langle \omega_3^2 \rangle^{1/2}$ in Figure 4. They are constructed using (14) for $N = 15$ (80%), $N = 42$ (90%) and $N = 264$ (99%) and compared with the exact profiles from the full simulation database. The vertical profile $\langle \omega\theta \rangle$ for $N = 264$ is indistinguishable from the exact profile as shown in Figure 4(a). Note that the convergence of the profiles appears to be uniform throughout the vertical interval. This is expected, because each K–L mode in the representation is associated with a basic flow, $\mathbf{v}^k$ of (10), carrying a full resolution of the numerical simulation in the inhomogeneous vertical direction. In the homogeneous horizontal directions the truncated K–L representation of the flow carries a selective range of wave numbers; for example, the representations capturing 80%, 90% and 99% of the energy involve the horizontal wave numbers $max\{|k_x|, |k_y|\} = 2$, 3 and 6 respectively.

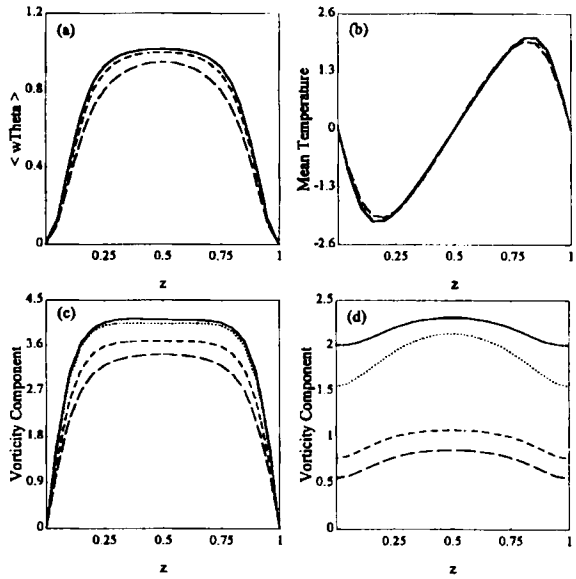

Figure 4. Convergence of vertical profiles of some flow quantities in K–L representation (– – –, $N = 15$; - · -, $N = 42$; $\cdots$, $N = 264$; —, exact): (a) $\langle w\theta \rangle$; (b) T^0; (c) $\langle \omega_1^2 \rangle^{1/2}$; (d) $\langle \omega_3^2 \rangle^{1/2}$

The mean component of the flow, namely the mean temperature T^0, can also be recovered through the K–L representation. This is achieved by expressing the mean temperature in terms of the fluctuating components of the flow. The ensemble averaging of (4c) provides such an expression in the form

$$\frac{d^2T^0}{dz^2} = \frac{d}{dz}\langle w\theta \rangle. \tag{15}$$

The mean temperature can be evaluated by integrating (15), after $\langle w\theta \rangle$ is known. The fast convergence of the $\langle w\theta \rangle$ profiles implies that T^0 can be recovered relatively well as shown in Figure 4(b) for the truncations under consideration.

5. DYNAMICAL APPROXIMATION

5.1. Formulation

It is of interest to study the K–L representation (10)–(12) in a dynamical environment. This is achieved through a spectral method[15,16] by approximating the flow fluctuation in a truncated K–L representation

$$\mathbf{v}' \approx \sum_{k=1}^{N} a_k(t)\boldsymbol{\psi}^k(\mathbf{x}) + a_{k^*}(t)\boldsymbol{\psi}^{k^*}(\mathbf{x}), \tag{16}$$

where the index k runs through the conjugate pairs, and substituting into (4), written symbolically for the flow fluctuation after the introduction of (7) as

$$\frac{\partial \mathbf{v}'}{\partial t} = \mathbf{D}(\mathbf{v}', T^0), \tag{17}$$

to obtain a semidiscrete approximation to (17) for the evolution of the retained modes in (16).

A separate treatment is required for the mean component of the flow in (17) and various strategies are proposed in Reference 6 for this purpose. The use of (15) for the simultaneous evaluation of the mean temperature requires an iterative procedure in the form of running time averaging in order to treat the ensemble average involved. We now propose a non-iterative procedure for the treatment of the mean component of the flow in a K–L-based dynamical approximation. To this end the temperature is decomposed into the mean and the fluctuation in the form

$$T = \overline{T} + \tau, \tag{18}$$

where the overbar indicates the horizontal average, so that

$$\overline{T} = \overline{T}(z, t) \quad \text{and} \quad \bar{\tau} = 0. \tag{19}$$

This decomposition is substituted into (4) to yield

$$\nabla \cdot \mathbf{u} = 0, \tag{20a}$$

$$\frac{\partial \mathbf{u}}{\partial t} + \mathbf{u}\cdot\nabla\mathbf{u} = -\nabla p + Ra\ Pr\ (\overline{T} + \tau)\mathbf{e}_z + Pr\ \Delta\mathbf{u}, \tag{20b}$$

$$\frac{\partial \tau}{\partial t} + \mathbf{u}\cdot\nabla\tau - \overline{\mathbf{u}\cdot\nabla\tau} + w\frac{\partial \overline{T}}{\partial z} = w + \Delta\tau \tag{20c}$$

for the fluctuation and

$$\frac{\partial \overline{T}}{\partial t} + \frac{\partial}{\partial z}\overline{w\tau} = \frac{\partial^2 \overline{T}}{\partial z^2} \tag{21}$$

for the mean component. The flow fluctuation $\mathbf{v}'$ now becomes

$$\mathbf{v}' = [\mathbf{u}, \tau]; \tag{22}$$

further, $\langle \mathbf{v}' \rangle = \mathbf{0}$ and $\langle \overline{T} \rangle = T^0(z)$. Finally, the procedure is completed by replacing (17) by (20) and (15) by (21), now involving only the horizontal averages in the previous deliberations.

As a result of the decomposition of the temperature into the mean and the fluctuation with a vanishing horizontal average in (18), the resulting flow $\mathbf{v}'$ in (22) does not contain the purely thermal $(0, 0, q)$ modes mentioned in Section 4.1. However, the evolution of these modes can be recovered by comparing the two decompositions of the temperature in (18) and (7), so that

$$\begin{aligned} \theta &= \overline{T} - T^0 + \tau \\ &= \overline{T} - \langle \overline{T} \rangle + \tau, \end{aligned} \tag{23}$$

and, since τ has a vanishing horizontal average, by

$$a_{(0,0,q)} = (\mathbf{v}, \boldsymbol{\psi}^{(0,0,q)}), \tag{24}$$

where

$$\mathbf{v} = [\mathbf{0}, \overline{T} - \langle \overline{T} \rangle]. \tag{25}$$

Thus the evolution of the family of purely thermal $(0, 0, q)$ modes is implicitly governed by (21).

5.2. Numerical procedure and results

A database has already been generated by the original simulation of the flow. This is used to numerically test the procedure outlined above and to demonstrate the effects of the truncated K–L representation of the flow in a dynamical environment. For this purpose the flow fluctuation $\mathbf{v}'$ in (22) is approximated in the form (16), in which $N = 264$ pairs of K–L modes are retained corresponding to the resolution of 99% of the energy. This results in a factor-of-45 ($\approx 3 \times 20^3/2 \times 264$) reduction in the number of degrees of freedom involved in the dynamical approximation in comparison with the original Fourier-based simulation. This particular order of truncation is chosen as a cut-off retaining comfortably the large-scale features of the flow, as follows from the discussion in Section 4.3.

In order to facilitate a later comparison, equations (20) and (21), after the introduction of the truncated K–L representation of the flow, are numerically integrated using the same numerical procedures as in the original simulation. The last sample in the original database is projected onto the retained K–L modes to provide the initial condition. A database of 500 time samples of expansion coefficients a_k of (16) and $\bar{T}$ of (18) is generated through sampling after a start-up phase. It is checked numerically that τ actually has a vanishing horizontal average at each instant of time.

The effect of the dynamical approximation on the retained K–L modes is shown in Figure 5, depicting the contribution of the retained modes to the energy of the flow in comparison with that of the corresponding K–L eigenvalues. Each is scaled by $\mathscr{E}_{264}$, where $\mathscr{E}_N = \sum_{k=1}^{N} \lambda_k$. There is an overall increase of about 3% in the total contributions of the retained K–L modes in the dynamical approximation when compared with $\mathscr{E}_{264}$. This is consistent with the physical picture[17] in that, since the dissipative effects of the truncated modes due to their non-linear interactions with the retained modes are absent, the flow compensates by dissipating more energy in the retained modes by increasing the energy of the modes.

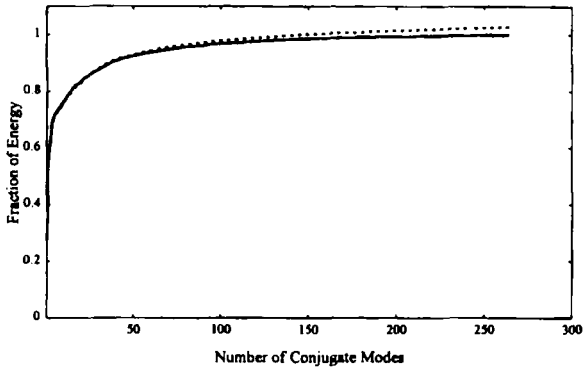

Figure 5. Fraction of energy content in K–L representation as a result of direct projection (—) and dynamical approximation with $N = 264(\cdots)$

The large-scale features of the flow are not affected, as inspection of the vertical profiles $\langle w\theta \rangle$ and T^0 in Figures 6(a) and 6(b) indicates. The profiles are constructed using the database resulting from the dynamical approximation and using the original database by retaining the same number of conjugate K–L mode pairs, namely $N = 264$. The root mean square profiles of vorticity, $\langle \omega_1^2 \rangle^{1/2}$ and $\langle \omega_3^2 \rangle^{1/2}$, on the other hand, are altered as shown in Figures 6(c) and 6(d). This suggests that the effect of the increased energy content of the retained K–L modes as a result of the dynamical approximation is felt mainly by the higher-order modes in the representation. This is consistent with the scale separation property of the K–L representation and the expectation that in the absence of the dissipative effects of the truncated modes the energy cascading down the scales accumulates closer to cut-off.

Energy does not constitute a sufficient criterion to determine those modes that are not dynamically significant enough to be included in the dynamical approximation. Table II gives the energy $\mathscr{E}$ and the

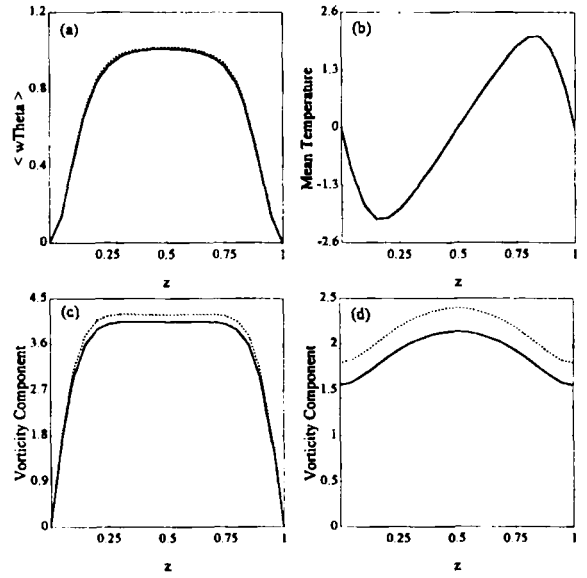

Figure 6. Vertical profiles of some flow quantities in K–L representation as a result of direct projection (—, $N = 264$) and dynamical approximation $(\cdots, N = 264)$: (a) $\langle w\theta \rangle$; (b) T^0; (c) $\langle \omega_1^2 \rangle^{1/2}$; (d) $\langle \omega_3^2 \rangle^{1/2}$

Table II. Total contributions of K–L modes to energy $\mathscr{E}$ and production and dissipation in exact and truncated representations of flow with $N = 264$

	Energy	Production	Dissipation
Exact	3·1441	6·4597	−6·4361
Truncated	3·1137	6·4419	−6·2504

quantities involved in the energy balance, namely production and dissipation defined as

$$\text{production} = \langle (Ra\ Pr\ T\mathbf{e}_z, \mathbf{u}) \rangle + \langle (w, T) \rangle, \tag{26}$$

$$\text{dissipation} = \langle (Pr\ \Delta\mathbf{u}, \mathbf{u}) \rangle + \langle (\Delta T, T) \rangle, \tag{27}$$

for the exact flow retaining all the modes and the truncated flow retaining $N = 264$ conjugate pairs of K–L modes. Note that the energy balance is not maintained in the truncated case and note also that the truncated modes contribute less than 1% to the production and around 3% to the dissipation. Since the production is insignificant, the energy to be dissipated in the truncated modes comes directly from the non-linear interactions of the truncated modes with the retained modes, which accounts for the 3% of the dissipation. It shows that those modes that are truncated, together with their non-linear interactions with the retained modes, are still dynamically active while not being significant from an energy point of view, contributing only 1% to the overall energy.

The above considerations confirm that if one is interested in recovering the large-scale features of the flow in a dynamical approximation, this can be achieved by utilizing the K–L basis, resulting in a large reduction of the size of the system. Furthermore, Figure 6(b) indicates the success of the proposed non-iterative procedure of recovering the mean temperature component in the dynamical approximation, since it shows an indistinguishable pair of mean temperature profiles.

6. DISCUSSION

Perhaps one of the important features of the K–L basis $\{\boldsymbol{\psi}^k\}$ is its carrying of the character of the flow, e.g. the vertical spatial structure and the symmetries that are built into the K–L eigenfunctions, rather than being a general basis for the space as is the case in the Fourier basis $\{\mathbf{V}^k\}$ in (6). This may be part of what enables the long-term integration of the evolution equations, which capture at least the large-scale features of the flow through the dynamical approximation involving the truncated K–L representation (16), by constantly reminding the flow of its character throughout the integration. The work presented here may constitute the outlines of a procedure in which a relatively short-term integration could be used to generate a database for the subsequent computation of the K–L eigenfunctions and they in turn are used in a dynamical approximation for the long-term integration. The question concerning the size of the database for the evaluation of the K–L eigenfunctions accurately characterizing the flow has been discussed in Reference 18.

In view of the dramatic effect of the truncation on the higher-order retained modes, a successful low-dimensional dynamical approximation requires the lost dissipative effects of the truncated modes to be somehow compensated, while keeping the size of the dynamical system small. An alternative technique to the introduction of an eddy viscosity, in order to compensate for the lost dissipative effects, is the so-called method of *slaved variables*. This can work suitably with an already optimally reduced dynamical system approximating (17) obtained through the Galerkin procedure utilizing the K–L basis. In this method a portion of the dynamical system is replaced by algebraic equations through

which the time evolution of the K–L modes associated with this portion is slaved to the modes whose time evolution is governed by the remaining portion of the dynamical system. A variation of this procedure is applied to the Ginzburg–Landau equation in Reference 8, in which the split into portions is made on the basis of so-called *acceleration* energy. The application of this procedure to the Rayleigh–Bénard problem is presently being carried out.

The K–L basis can be further utilized to explore its usefulness over a range of parameter values such as the Rayleigh number which are different from those reference values at which the basis is generated. As suggested in Reference 6, the basis is not expected in general to enjoy properties such as the optimal representation of the flow and the statistical orthogonality (3) of its expansion coefficients a_k when it is in use for off-reference values of the parameters. However, it will still form a complete orthogonal set satisfying the boundary conditions and the continuity. It has been applied to the Ginzburg–Landau equation in Reference 3 and its application to the Rayleigh–Bénard problem is currently under investigation. This application can be further facilitated by the use of the presently suggested treatment of the mean component of the flow in Section 5 to account for its variation with the parameter values.

ACKNOWLEDGEMENTS

The computation in this work was carried out at the Pittsburgh Supercomputing Center, Pittsburgh, PA and at the Data Processing Center of King Fahd University of Petroleum and Minerals, Dhahran. The author also gratefully acknowledges the support given by Lawrence Sirovich.

REFERENCES

1. A. Papoulis, *Probability, Random Variables and Stochastic Processes*, McGraw-Hill, New York, 1965.
2. L. Sirovich, M. Maxey and I. H. Tarman, 'An eigenfunction analysis of turbulent thermal convection', in B. E. Launder (ed), *Proc. 6th. Symp. on Turbulent Shear Flows*, Springer, New York, 68, 1989.
3. L. Sirovich and J. D. Rodriguez, 'Coherent structures and chaos: a model problem', *Phys. Lett. A*, **120**, 211 (1987).
4. N. Aubry, P. Holmes, J. L. Lumley and E. Stone, 'The dynamics of coherent structures in the wall region of a turbulent boundary layer', *J. Fluid Mech.*, **192**, 115–173 (1988).
5. J. L. Lumley, 'The structure of inhomogeneous turbulent flows', in A. M. Yaglom and V. I. Tatarski (eds), *Atmospheric Turbulence and Radio Wave Propogation*, Nauka, Moscow, 166, 1967.
6. L. Sirovich, 'Turbulence and the dynamics of coherent structures, Parts I–III', *Q. Appl. Math.*, **45**, 561 (1987).
7. M. Kirby, 'Minimal dynamical systems from PDEs using Sobolev eigenfunctions', *Physica D*, **57**, 466–475 (1992).
8. L. Sirovich, B. W. Knight and J. D. Rodriguez, 'Optimal low-dimensional dynamical approximations', *Q. Appl. Math.*, **48**, 535 (1990).
9. A. N. Deane and L. Sirovich, 'A computational study of Rayleigh–Bénard convection. Part 1. Rayleigh-number scaling', *J. Fluid Mech.*, **222**, 231–250 (1991).
10. J. H. Curry, J. R. Herring, J. Loncaric and S. A. Orszag, 'Order and disorder in two- and three-dimensional Bénard convection', *J. Fluid Mech.*, **147**, 1–38 (1984).
11. P. G. Drazin and W. H. Reid, *Hydrodynamic Stability*, Cambridge University Press, Cambridge, 1985.
12. F. H. Busse, 'The oscillatory instability of convection rolls in a low Prandtl number fluid', *J. Fluid Mech.*, **52**, 97–112 (1972).
13. P. Moin and R. D. Moser, 'Characteristic-eddy decomposition of turbulence in a channel', *J. Fluid Mech.*, **200**, 471–509 (1989).
14. D. H. Chambers, R. J. Adrian, P. Moin, D. S. Stewart and H. J. Sung, 'Karhunen–Loève expansion of Burgers' model of turbulence', *Phys. Fluids*, **31**, 2573–2582 (1988).
15. C. Canuto, M. Y. Hussaini, A. Quarteroni and T. A. Zang, *Spectral Methods in Fluid Dynamics*, Springer, New York, 1987.
16. D. Gottlieb and S. A. Orszag, *Numerical Analysis of Spectral Methods: Theory and Applications*, SIAM–CBMS, Philadelphia, PA, 1977.
17. P. S. Marcus, 'Effects of truncation in modal representations of thermal convection', *J. Fluid Mech.*, **103**, 241–255 (1981).
18. L. Sirovich, 'Empirical eigenfunctions and low dimensional systems', in L. Sirovich (ed), *New Perspectives in Turbulence*, Springer, New York, 139, 1991.